Journal of Modern Optics

ISSN: 0950-0340 (Print) 1362-3044 (Online) Journal homepage: http://www.tandfonline.com/loi/tmop20

Linearized inversion methods for three-dimensional electromagnetic imaging in the multiple scattering regime

Kevin Unger, Ting Zhang, Patrick C. Chaumet, Anne Sentenac & Kamal Belkebir

To cite this article: Kevin Unger, Ting Zhang, Patrick C. Chaumet, Anne Sentenac & Kamal Belkebir (2018) Linearized inversion methods for three-dimensional electromagnetic imaging in the multiple scattering regime, Journal of Modern Optics, 65:15, 1787-1792, DOI: 10.1080/09500340.2018.1459912

To link to this article: https://doi.org/10.1080/09500340.2018.1459912

JOURNAL OF MODERN OPTICS, 2018
VOL. 65, NO. 15, 1787–1792
https://doi.org/10.1080/09500340.2018.1459912

Taylor & Francis
Taylor & Francis Group

Linearized inversion methods for three-dimensional electromagnetic imaging in the multiple scattering regime

Kevin Unger[a], Ting Zhang[b], Patrick C. Chaumet[a], Anne Sentenac[a] and Kamal Belkebir[a]

[a]Aix Marseille Université, CNRS, Centrale Marseille, Institut Fresnel, UMR 7249, Marseille, France; [b]Key Laboratory of Ocean Observation-Imaging Testbed of Zhejiang Province, College of Information Science and Electronic Engineering (ISEE), Zhejiang University, Hangzhou, China

ABSTRACT

In optical or microwave computational tomography, the sample permittivity is reconstructed numerically from the measurements of its scattered field for various illuminations. When the light sample interaction involves multiple scattering, the relationship between the scattered field and the permittivity is non-linear and a direct reconstruction is not possible. Using a simple physical approach, adapted to the three-dimensional vectorial electromagnetic framework, we derive an iterative inversion technique, based on the linearization of the scattering operator, for imaging (possibly anisotropic) targets in the multiple scattering regime. We investigate the performances of different approximations of this operator accounting for more or less multiple scattering. Our method is applied to the reconstruction of targets in the microwave domain using experimental data.

ARTICLE HISTORY
Received 1 December 2017
Accepted 10 March 2018

KEYWORDS
Inverse problem; vectorial scattering

1. Introduction

Fostered by the continuous improvement of computer capacity, the last 20 years have seen the rise of computational electromagnetic imaging, first in the microwave domain and more recently in optics. This imaging approach is based on an accurate modelling of the link between the recorded field and the sample permittivity and the use of an inverse technique for reconstructing the sample from the data. When the sample is weakly contrasted, the measurements are usually assumed to be linearly linked to the sample permittivity and standard direct or iterative linear inverse methods are applied to the data. When the sample supports multiple scattering, the recorded field is no more linearly linked to the sought sample permittivity distribution and the reconstruction procedure must grope its way towards a solution. The classical technique, which belongs to the linearized inversion schemes (*1*), consists in estimating iteratively the sample permittivity so as to minimize the distance (or cost functional) between the data and the field simulated for a given sample estimation. In most cases, the minimization is performed using a gradient technique. Now the derivation of the gradient of the cost functional with respect to the permittivity is not straightforward when multiple scattering is present. In practice, only a few studies have addressed the issue in the case of 3D electromagnetic imaging. Expressions obtained from the Lagrangian approach (*2*) or from a direct derivation of the cost functional (*3*–*6*) have thus been proposed but the complexity of their formulations hinders their comparison.

In this paper, we present a simple physic-based technique to derive the gradient in the complex configuration of 3D vectorial electromagnetic imaging of anisotropic targets. A similar approach has been used, in acoustic imaging, to provide an expression that is equivalent to that given by the Lagrangian multiplier or the direct derivation (*7*). The easy physical interpretation of the gradient permits to investigate several approximations accounting for more or less multiple scattering that are numerically more tractable. The performance of the different approximations in a standard conjugate-gradient inversion scheme are analysed on experimental microwave data.

2. The inverse problem context

We consider a target defined by its permittivity distribution $\overline{\varepsilon}$. To be as general as possible, the target permittivity may be anisotropic as long as it is reciprocal. In other words, $\overline{\varepsilon}$ is a tensor satisfying ${}^t\overline{\varepsilon} = \overline{\varepsilon}$, where ${}^t\overline{\varepsilon}$ is the transpose of the tensor $\overline{\varepsilon}$. The imaging problem consists in estimating $\overline{\varepsilon}$ in a domain under investigation Ω from the measurements $\mathcal{M}$ of the electromagnetic field taken for various observation and source positions $(\mathbf{o}, \mathbf{s}) \in \Gamma$. We call $\mathcal{E}[\overline{\varepsilon}](\mathbf{o}, \mathbf{s})$ the model of the recorded data, for a

CONTACT Anne Sentenac anne.sentenac@fresnel.fr

given observation and illumination pair, which depends on $\overline{\varepsilon}$. The inverse problem consists in finding $\overline{\varepsilon}$ such that,

$$\mathcal{M} = \mathcal{E}[\overline{\varepsilon}]. \tag{1}$$

The Maxwell equations that describe the interaction between an electromagnetic wave and an inhomogeneous medium yield a forward model $\mathcal{E}(\overline{\varepsilon})$ which is generally nonlinear with respect to $\overline{\varepsilon}$. In this case, the estimation of $\overline{\varepsilon}$ satisfying Equation (1) is not straightforward. The simplest approach from a conceptual point of view consists in minimizing iteratively the error $\mathcal{M} - \mathcal{E}(\overline{\varepsilon})$ by modifying the permittivity $\overline{\varepsilon}$ with a small perturbation $\overline{\delta\varepsilon}$, using

$$\mathcal{E}[\overline{\varepsilon} + \overline{\delta\varepsilon}] - \mathcal{E}[\overline{\varepsilon}] = \mathcal{D}[\overline{\delta\varepsilon}] + o(\overline{\delta\varepsilon}), \tag{2}$$

where $\mathcal{D}$ is a linear operator (known as the Fréchet operator) which transforms an Ω-tensor into a Γ-function. For each iteration step, the estimation of $\overline{\delta\varepsilon}$ minimizing $\mathcal{M} - \mathcal{E}[\overline{\varepsilon}] - \mathcal{D}[\overline{\delta\varepsilon}]$ is obtained with a standard linear inversion scheme (*8*). This technique is very expensive numerically and more tractable methods in which $\overline{\delta\varepsilon}$ is sought along a particular direction $\overline{u}$ are often preferred. In these approaches, $\overline{\delta\varepsilon}$ is written as $\overline{\delta\varepsilon} = \alpha\overline{u}$ and the scalar α only is optimized. The search direction $\overline{u}$ is usually built from the gradient of a cost functional $\mathcal{F}(\overline{\varepsilon})$ representing the distance between the data and the model with respect to $\overline{\varepsilon}$. To define this distance, one introduces an inner product on Γ,

$$\langle e, f \rangle_\Gamma = \sum_{(\mathbf{o},\mathbf{s})\in\Gamma} e^*(\mathbf{o},\mathbf{s}) f(\mathbf{o},\mathbf{s}), \tag{3}$$

where a^* stands for the conjugate of a, so that $\mathcal{F}(\overline{\varepsilon})$ reads,

$$\mathcal{F}(\overline{\varepsilon}) \propto \|\mathcal{M} - \mathcal{E}[\overline{\varepsilon}]\|_\Gamma^2 = \|h\|_\Gamma^2, \tag{4}$$

where $h(\mathbf{o},\mathbf{s}) = \mathcal{M}(\mathbf{o},\mathbf{s}) - \mathcal{E}[\overline{\varepsilon}](\mathbf{o},\mathbf{s})$ denotes the residual error computed from Equation (1). Recalling that the gradient $\overline{g}$ is the vector $\overline{u}$ in Ω that maximizes the directional derivative

$$\lim_{t\to 0} \frac{\mathcal{F}(\overline{\varepsilon} + t\overline{u}) - \mathcal{F}(\overline{\varepsilon})}{t}, \tag{5}$$

one easily finds that

$$\overline{g} = -\mathcal{D}^\dagger[h], \tag{6}$$

where the adjoint operator $\mathcal{D}^\dagger$ is defined as, $\langle \mathcal{D}^\dagger[e], \overline{\eta} \rangle_\Omega = \langle e, \mathcal{D}[\overline{\eta}] \rangle_\Gamma$, with the Frobenius inner product over Ω

$$\left\langle \overline{e}, \overline{f} \right\rangle_\Omega = \int_\Omega \overline{e}^*(\mathbf{r}) : \overline{f}(\mathbf{r}) \mathrm{d}\mathbf{r}, \tag{7}$$

where $\overline{a} : \overline{b} = \sum_{ij} a_{ij} b_{ij}$ in an orthogonal basis representation.

The Fréchet operator, which linearizes the scattering problem, is thus a key issue of most inversion schemes. In the following, we derive its expression in the general framework of electromagnetic scattering by anisotropic inhomogeneous media.

3. Derivation of the Fréchet operator

We consider an imaging configuration where the target is illuminated by a monochromatic dipole antenna $\mathbf{p}_s$ located at the position $\mathbf{s}$ and the recorded data correspond to the electric field observed at the observation point $\mathbf{o}$ projected onto the observation dipole antenna $\mathbf{p}_o$. We start from a reference inhomogeneous medium described by its reciprocal permittivity tensor $\overline{\varepsilon}$. We call $\mathbf{E}_\varepsilon(\mathbf{r},\mathbf{s})$ the electric field observed at $\mathbf{r}$ in the reference medium, radiated by a monochromatic dipole $\mathbf{p}_s$ located at the position $\mathbf{s}$ and $\overline{\mathbf{G}}$ the monochromatic Green tensor of the medium. By definition, $\mathbf{E}_\varepsilon(\mathbf{r},\mathbf{s}) = \overline{\mathbf{G}}(\mathbf{r},\mathbf{s})\mathbf{p}_s$. We now introduce a permittivity fluctuation $\overline{\delta\varepsilon}$ in the domain under investigation Ω. According to the volume integral equation stemming from Maxwell equations (*9*), the field in the perturbed medium created by the source $\mathbf{p}_s$, $\mathbf{E}_{\varepsilon+\delta\varepsilon}(\mathbf{r},\mathbf{s})$, can be written as the field in the reference medium $\mathbf{E}_\varepsilon(\mathbf{r},\mathbf{s})$ plus the field radiated by the induced sources $\overline{\delta\varepsilon}\mathbf{E}_{\varepsilon+\delta\varepsilon}$,

$$\mathbf{E}_{\varepsilon+\delta\varepsilon}(\mathbf{r},\mathbf{s}) = \mathbf{E}_\varepsilon(\mathbf{r},\mathbf{s}) + \int_\Omega \overline{\mathbf{G}}(\mathbf{r},\mathbf{r}')\overline{\delta\varepsilon}(\mathbf{r}')\mathbf{E}_{\varepsilon+\delta\varepsilon}(\mathbf{r}',\mathbf{s})\mathrm{d}\mathbf{r}'. \tag{8}$$

Taking $\mathbf{r} = \mathbf{o} \in \Gamma$ and projecting the field on the observation antenna $\mathbf{p}_o$ yield the data model,

$$\mathcal{E}[\overline{\varepsilon} + \overline{\delta\varepsilon}](\mathbf{o},\mathbf{s}) = \mathcal{E}[\overline{\varepsilon}](\mathbf{o},\mathbf{s}) + \int_\Omega \mathbf{p}_o \cdot \overline{\mathbf{G}}(\mathbf{o},\mathbf{r})\overline{\delta\varepsilon}(\mathbf{r})\mathbf{E}_{\varepsilon+\delta\varepsilon}(\mathbf{r},\mathbf{s})\mathrm{d}\mathbf{r}. \tag{9}$$

The reciprocity theorem (*10*), valid in a reciprocal inhomogeneous medium, $\mathbf{u}\cdot\overline{\mathbf{G}}(\mathbf{r}_u,\mathbf{r}_v)\mathbf{v} = \mathbf{v}\cdot\overline{\mathbf{G}}(\mathbf{r}_v,\mathbf{r}_u)\mathbf{u}$, permits to rewrite Equation (9) as,

$$\mathcal{E}[\overline{\varepsilon} + \overline{\delta\varepsilon}](\mathbf{o},\mathbf{s}) - \mathcal{E}[\overline{\varepsilon}](\mathbf{o},\mathbf{s}) = \int_\Omega \overline{\delta\varepsilon}(\mathbf{r})\mathbf{E}_{\varepsilon+\delta\varepsilon}(\mathbf{r},\mathbf{s}) \cdot \mathbf{E}_\varepsilon(\mathbf{r},\mathbf{o})\mathrm{d}\mathbf{r}, \tag{10}$$

where $\mathbf{E}_\varepsilon(\mathbf{r},\mathbf{o}) = \overline{\mathbf{G}}(\mathbf{r},\mathbf{o})\mathbf{p}_o$ is the field observed at $\mathbf{r}$ in the reference medium generated by the antenna $\mathbf{p}_o$ located at the position $\mathbf{o}$. Subtracting Equation (8) in the right-hand term of Equation (10), one can build a series in all orders of $\overline{\delta\varepsilon}$ whose first term yields the Fréchet operator (and the second term is the Hessian),

$$\mathcal{D}[\overline{\delta\varepsilon}](\mathbf{o},\mathbf{s}) = \int_{\Omega} \overline{\delta\varepsilon}(\mathbf{r})\mathbf{E}_{\varepsilon}(\mathbf{r},\mathbf{s})\cdot\mathbf{E}_{\varepsilon}(\mathbf{r},\mathbf{o})\mathrm{d}\mathbf{r},$$
$$\mathcal{D}(\mathbf{o},\mathbf{s},\mathbf{r})\overline{\delta\varepsilon}(\mathbf{r}) = \left[\mathbf{E}_{\varepsilon}(\mathbf{r},\mathbf{o})\otimes\mathbf{E}_{\varepsilon}(\mathbf{r},\mathbf{s})\right] : \overline{\delta\varepsilon}(\mathbf{r}). \quad (11)$$

Equation (11) shows that the estimation of the Fréchet operator and the related gradient requires only the calculation of two fields in the reference medium, one generated by an emitter located at the source position **s** and one generated by an emitter located at the observation position **o**.

4. Reconstruction of targets

To compare our formulation to the gradients given in the literature, we consider an imaging problem in which the targets are made of isotropic materials (the sought permittivity is a scalar) and the source and observation antennas ($\mathbf{p}_s$, $\mathbf{p}_o$) belong to fixed independent domains Γ_s and Γ_o with N_s and N_o points, respectively. In this case, the Fréchet operator transforming a function of $\mathbf{r}\in\Omega$ in a function of $(\mathbf{o},\mathbf{s})\in\Gamma$ reads, $\mathcal{D}(\mathbf{o},\mathbf{s},\mathbf{r}) = \mathbf{E}_{\varepsilon}(\mathbf{r},\mathbf{s})\cdot\mathbf{E}_{\varepsilon}(\mathbf{r},\mathbf{o})$ and the gradient given by Equation (6) reads,

$$g(\mathbf{r}) = -\sum_{\mathbf{s}\in\Gamma_s}\mathbf{E}^{*}_{\varepsilon}(\mathbf{r},\mathbf{s})\cdot\left[\sum_{\mathbf{o}\in\Gamma_o}\mathbf{E}^{*}_{\varepsilon}(\mathbf{r},\mathbf{o})h(\mathbf{o},\mathbf{s})\right]. \quad (12)$$

The expression 12 is similar to that obtained with the Lagrange multiplier (*2*). It is the dot product of two near-fields in the medium of permittivity ε, one stemming from the emitter $\mathbf{p}_s$ and one stemming from a source located at the observation points, $\mathbf{S}_s(\mathbf{r}) = \sum_{\mathbf{o}\in\Gamma_o} h(\mathbf{o},\mathbf{s})\mathbf{p}_o\,\delta(\mathbf{r}-\mathbf{o})$. These $2N_s$ electric fields can be computed with any Maxwell equation solver (*9*). Yet, if the domain under investigation is large, this rigorous calculation can be time consuming and the use of approximate models for estimating the fields in Equations (12) and (4) (Born (*11*), Rytov (*12*), Beam Propagation Method (*13*) among others) may be interesting.

In the following, we investigate the performance of different gradient approximations in a standard conjugate gradient inversion scheme (*3*) applied to the reconstruction of targets in the microwave domain.

For an arbitrary permittivity $\varepsilon(\mathbf{r})$, the field $\mathbf{E}(\mathbf{r})$ is computed at any position **r** of the domain under investigation Ω with the method of moments (*14*, *15*) which consists in discretizing Equation (8); Ω is split into elemental units little enough so that the Green function $\overline{\mathbf{G}}$, the permittivity ε and the field **E** can be assumed constants inside each unit: the computation of the field is reduced to the resolution of a linear system with the value of the field at the different units as unknowns. Many standard linear solvers exists and we use a biconjugate gradient method to compute quickly and with accuracy the field (*16*).

The algorithm implemented in this study minimizes the distance

$$\mathcal{F}(\varepsilon) = \frac{\sum_l \|\mathbf{E}^{\mathrm{mes}}_l - \mathbf{E}^{\mathrm{d}}_l(\varepsilon)\|^2_{\Gamma_o}}{\sum_l \|\mathbf{E}^{\mathrm{mes}}_l\|^2_{\Gamma_o}}, \quad (13)$$

between the measured detected field $\mathbf{E}^{\mathrm{mes}}$ and the detected field $\mathbf{E}^{\mathrm{d}}(\varepsilon)$ that would be computed for a sample of permittivity ε with the scattering model. The minimization is performed thanks to a classical gradient technique which updates iteratively ε with the relation

$$\varepsilon_n = \varepsilon_{n-1} + \alpha_n d_n, \quad (14)$$

where d_n is the Polak-Ribiére descent

$$d_n = g_n + a_{n,\varepsilon} d_{n-1}, \quad (15)$$

with

$$a_{n,\varepsilon} = \frac{< g_n | g_n - g_{n-1} >_{\Omega}}{\|g_{n-1}\|^2_{\Omega}}, \quad (16)$$

and g_n is computed with Equation (12); and α_n is a real number which minimizes the cost functional $\mathcal{F}$ at the next iteration.

Among the various approximations possible to compute the fields in the gradient $g(\mathbf{r})$, we consider only the Born approximation and the rigorous calculation to distinguish clearly the two states, accounting thoroughly or not at all for multiple scattering. In addition, we do not use any regularization to avoid any bias in the comparisons. In all cases, Equation (4) is evaluated using a rigorous calculation of $\mathcal{E}[\overline{\varepsilon}]$.

The first approximation, called Born-Born, consists in supposing that $\overline{\varepsilon}(\mathbf{r}) - 1$ is small enough for $\mathbf{E}_{\varepsilon}$ to be close to the field existing in vacuum $\mathbf{E}_{\mathrm{vac}}$. This approximation, amounts to overlooking any perturbation induced by $\overline{\varepsilon}$, and thus any possible multiple scattering in the estimation of the Fréchet operator. The expression of $\mathbf{E}_{\mathrm{vac}}$ being analytically, the calculation is quasi-instantaneous.

The second approximation, called Born-Rig, accounts for some multiple-scattering. It still replaces $\mathbf{E}_{\varepsilon}(\mathbf{r},\mathbf{o})$ by $\mathbf{E}_{\mathrm{vac}}(\mathbf{r},\mathbf{o})$ but it calculates rigorously $\mathbf{E}_{\varepsilon}(\mathbf{r},\mathbf{s})$. This choice is dictated by the fact that a rigorous calculation of $\mathbf{E}_{\varepsilon}(\mathbf{o},\mathbf{s})$ is anyway necessary for estimating the residue, Equation (4), and the near-field in Ω, $\mathbf{E}_{\varepsilon}(\mathbf{r},\mathbf{s})$, is an easy to get by-product of this computation. This is particularly true if one uses a volume integral method (*9*). This approximation can be found in several studies (*3*). From a computational point of view, the Born-Rig approximation, requires the solving of N_s forward problems at each iteration of the algorithm.

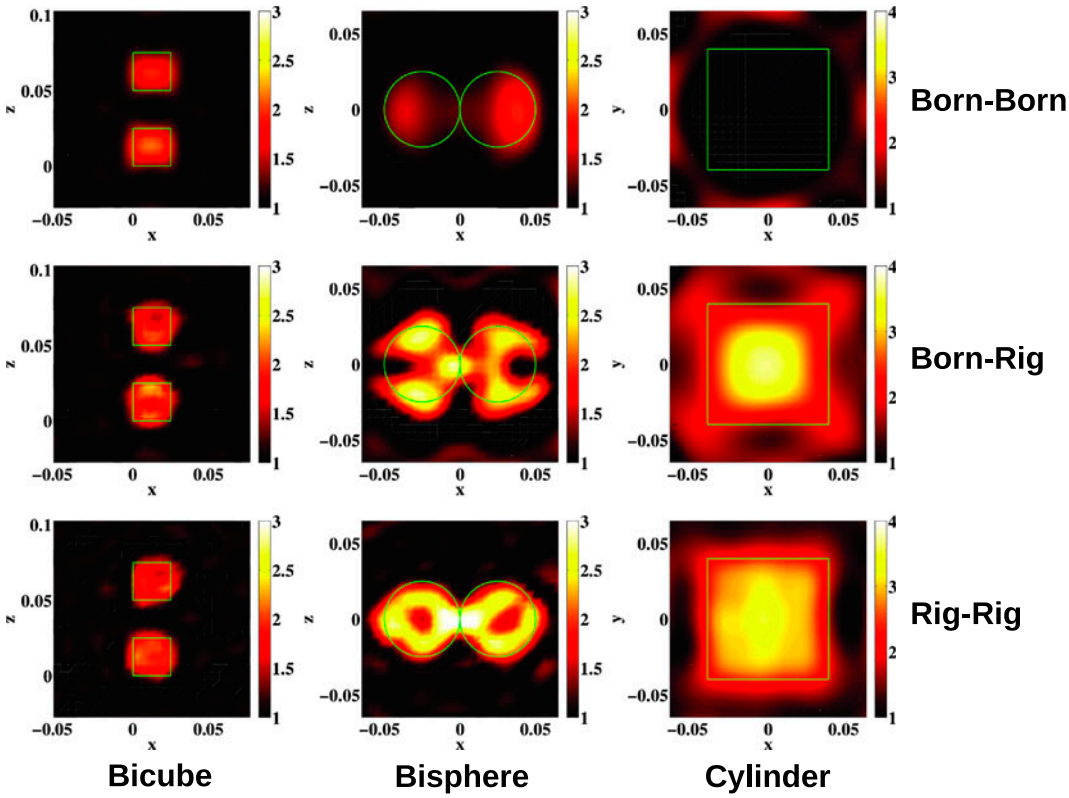

Figure 1. Target reconstructions using three different expressions for the gradient. The units of the figure are in centimeter. (*left column*) two cubes with edge $a = 2.5$ cm and $\varepsilon = 2.4$ at 8 GHz ($\lambda = 3.75$ cm); (*center column*) two touching spheres with radius $r = 2.5$ cm and $\varepsilon = 2.6$ at 5 GHz ($\lambda = 6$ cm); (*right column*) a circular-basis cylinder with radius $r = 4$ cm, height $h = 8$ cm and $\varepsilon = 3.05$ at 3 GHz ($\lambda = 10$ cm). The (*first*), (*second*) and (*third line*) correspond to the reconstructions with Born-Born, Born-Rig and Rig-Rig gradients, respectively. The solid line indicates the exact contour of the real object. For each case except Born-Born Cylinder and Born-Rig Cylinder, the 100th iteration is shown from which the cost functional reaches a plateau. For the cylinder, however, the multiple scattering is so strong inside the sample that the cost functional diverges after the 5th iteration under the Born-Born approximation and shows a chaotic evolution under the Born-Rig approximation. The 5th iteration under the Born-Born approximation is shown. The 63th iteration under the Born-Rig approximation where the cost functional reaches its lowest value is shown. For more details about the convergence of the cost functional, see Figure 2.

The third evaluation of the gradient, called Rig-Rig, corresponds to the rigorous calculation and it requires the solving of $2N_s$ forward problems at each iteration.

We study the effectiveness of the three approximations previously described in the reconstruction process thanks to the Fresnel database. The database provides experimental scattered fields associated to different targets with low, moderate and strong multiple scattering. The imaging configuration is thoroughly described in Refs. (*17*–*19*). Each target of the database is illuminated by 81 polarized antennas and the complex amplitude of the scattered field is collected on 36 observation antennas. The antennas are distributed on a sphere of radius 1.796 m with the target at the center. The precise positions of the source and receiver antennas are described in Sections 2.3 *Sources locations* and 2.4 *Receiver locations* in Ref. (*17*). The scattered fields have been measured at different illuminating frequencies ranging from 3 to 8 GHz. The measurements have been performed in an electromagnetic anechoic chamber and the target position was far from any dielectric dioptres. With these experimental precautions, the free space configuration can be assumed. Among the different targets available, we choose to study three particular targets. The first target is composed of two identical cubes (edge 2.5 cm, relative permittivity 2.4) separated from each other of 2.5 cm along the z axis. The second target is composed of two identical balls (radius 2.5 cm, relative permittivity 2.6) in contact along the x axis. The third target is a cylinder with a circular basis (height 8 cm, radius 4 cm, relative permittivity 3.05) oriented along the x axis. The bicube, the bisphere and the cylinder show increasing scattering capacities and multiple scattering.

Since the studied targets have been well characterized, we estimate the quadratic susceptibility error $\mathrm{Err}(\varepsilon) = \frac{\|\varepsilon - \varepsilon^{\mathrm{true}}\|^2_\Omega}{\|\varepsilon^{\mathrm{true}} - 1\|^2_\Omega}$ between the reconstructed permittivity with re-

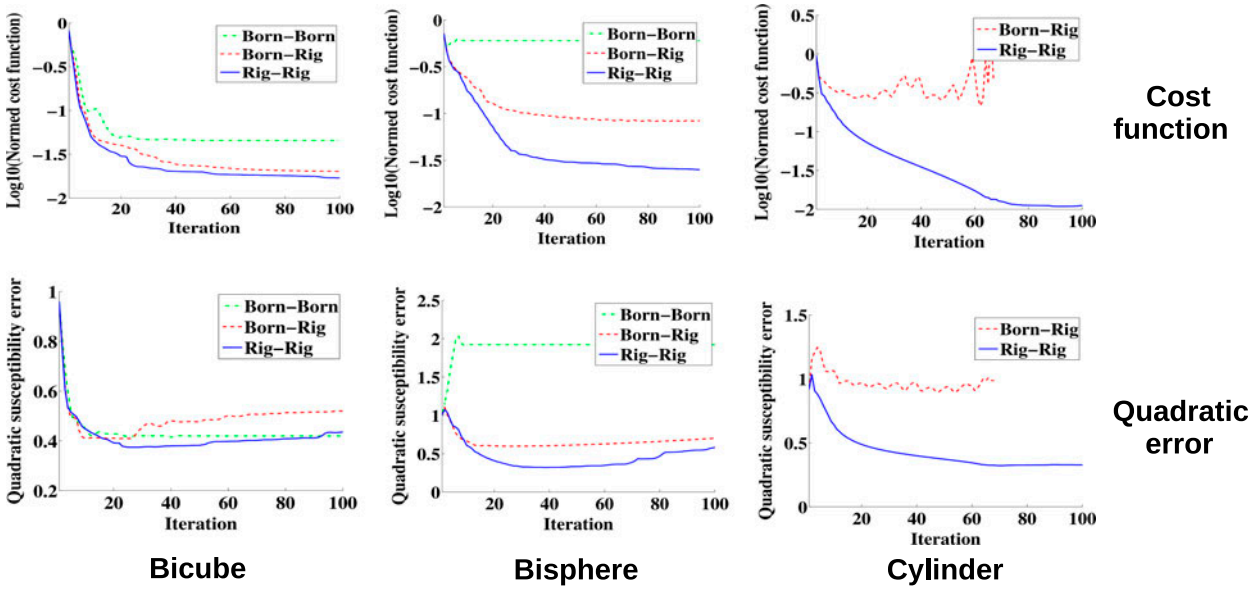

Figure 2. Evolution of the cost functional (*first line*) and of the quadratic susceptibility error $\frac{\|\varepsilon-\varepsilon^{\text{true}}\|^2_\Omega}{\|\varepsilon^{\text{true}}-1\|^2_\Omega}$ (*second line*) with respect to the iterations using three different expressions for the gradient. (*left column*) two cubes with edge $a = 2.5$ cm and $\varepsilon = 2.4$ at 8 GHz ($\lambda = 3.75$ cm); (*center column*) two touching spheres with radius $r = 2.5$ cm and $\varepsilon = 2.6$ at 5 GHz ($\lambda = 6$ cm); (*right column*) a circular-basis cylinder with radius $r = 4$ cm, height $h = 8$ cm and $\varepsilon = 3.05$ at 3 GHz ($\lambda = 10$ cm).

spect to the real target permittivity $\varepsilon^{\text{true}}$ (Figure 2). When the targets are weakly scattering, Figure 1 (left column), the reconstruction obtained with the Born-Rig or even the Born-Born approximation is satisfactory (Err(ε) = 40%). When the targets support moderate multiple scattering, Figure 1 (center column), the influence of the different gradient approximations becomes visible : Born-Rig and Rig-Rig (Err(ε) = 50%) better estimate the high spatial frequencies of the dimer, especially at the contact point, than Born-Born (Err(ε) = 200%). When the object supports strong multiple scattering as in Figure 1(right column) the Rig-Rig reconstruction (Err(ε) = 40%) is significantly better than the Born-Rig one (Err (ε) = 100%) while the Born-Born algorithm diverges after the first iteration.

5. Conclusion

In conclusion, we have given a simple physics-based approach for deriving an iterative inversion scheme adapted to electromagnetic imaging in the multiple scattering regime. We have investigated the performance of different search strategies under the conditions of weak and strong multiple scattering. We have shown that a rigorous evaluation of these directions, requiring the solving of many forward problems, is not always necessary. This study paves the way to the development of approximate iterative inversion techniques that are less time consuming in the moderate multiple scattering regime.

Disclosure statement

No potential conflict of interest was reported by the authors.

References

(1) Mudry, E.; Chaumet, P.C.; Belkebir, K.; Sentenac, A. Electromagnetic Wave Imaging of Three-dimensional Targets Using a Hybrid Iterative Inversion Method. *Inverse Probl.* **2012,** *28,* 065007.
(2) Voznyuk, I.; Litman, A.; Tortel, H. Efficient Combination of a 3d Quasi-Newton Inversion Algorithm and a Vector Dual-primal Finite Element Tearing and Interconnecting Method. *Inverse Probl.* **2015,** *31,* 085005.
(3) Chaumet, P.C.; Belkebir, K. Three-dimensional Reconstruction from Real Data Using a Conjugate Gradient-coupled Dipole Method. *Inverse Probl.* **2009,** *25,* 024003–17.
(4) De Zaeytijd, J.; Franchois, A. Three-dimensional Quantitative Microwave Imaging from Measured Data with Multiplicative Smoothing and Value Picking Regularization. *Inverse Probl.* **2009,** *25,* 024004.
(5) Yuan, M.; Yu, C.; Liu, Q.H. Reconstruction of 3D Objects from Multi-frequency Experimental Data with a Fast DBIM-BCGS Method. *Inverse Probl.* **2009,** *25,* 024007–24.
(6) Soubies, E.; Pham, T.-A.; Unser, M. Efficient Inversion of Multiple-scattering Model for Optical Diffraction Tomography. *Optics Exp.* **2017,** *25* (Aug), 21786.
(7) Norton, S.J. Iterative Inverse Scattering Algorithms: Methods Of Computing Fréchet Derivatives. *J. Acoust. Soc. Amer.* **1999,** *106,* 2653–2660.

(8) Roger, A. Newton-Kantorovitch Algorithm Applied to an Electromagnetic Inverse Problem. *IEEE Trans. Antennas Propag.* **1981,** *29,* 232–238.
(9) Kahnert, F.M. Numerical Methods in Electromagnetic Scattering Theory. *J. Quant. Spect. Rad. Transf.* **2003,** *79–80,* 775–824.
(10) Van Bladel, J.G. *Electromagnetic Fields, 2nd Edition*. IEEE Press Ser. Electromagn. Wave Theory, IEEE Press: Wiley, **2007**.
(11) Wolf, E. Three-dimensional Structure Determination of Semi-transparent Objects from Holographic Data. *Opt. Commun.* **1969,** *1,* 153–156.
(12) Carminati, R. Phase Properties of the Optical Near Field. *Phys. Rev. E* **1997,** *55*(May), R4901–R4904.
(13) Liu, J.M.; Gomelsky, L. Vectorial Beam Propagation Method. *J. Opt. Soc. Amer. A* **1992,** *9* (Sep), 1574.
(14) Draine, B.T.; Flatau, P.J. Discrete-dipole Approximation for Scattering Calculations. *J. Opt. Soc. Am. A* **1994,** *11,* 1491–1499.
(15) Chaumet, P.C.; Sentenac, A.; Rahmani, A. Coupled Dipole Method for Scatterers with Large Permittivity. *Phys. Rev. E* **2004,** *70,* 036606–6.
(16) Chaumet, P.C.; Rahmani, A. Efficient Iterative Solution of the Discrete Dipole Approximation for Magneto-dielectric Scatterers. *Opt. Lett.* **2009,** *34,* 917–919.
(17) Geffrin, J.M.; Sabouroux, P. Continuing with the Fresnel Database: Experimental Setup and Improvements in 3D Scattering Measurements. *Inverse Probl.* **2009,** *25,* 024001.
(18) Eyraud, C. J.-M geffrin, A. Litman, P. Sabouroux, and H. Giovannini. Drift Correction for Scattering Measurements. *Appl. Phys. Lett.* **2006,** *89,* 244104.
(19) Eyraud, C.; Geffrin, J.M.; Sabouroux, P.; Chaumet, P.C.; Tortel, H.; Giovannini, H.; Litman, A. Validation of 3D Bistatic Microwave Scattering Measurement Setup. *Radio Sci* **2008,** *43,* RS4018.